Feature Article:

DOI. No. 10.1109/MAES.2022.3178664

Opportunistic Autonomous Integrity Monitoring for Enhanced UAV Safety

Joe Khalife, Mahdi Maaref, and Zaher M. Kassas, **University of California, Irvine, CA 92697 USA**

INTRODUCTION

Autonomous unmanned aerial vehicles (UAVs) are predicted to revolutionize a wide range of sectors, such as surveying, farming, filming, construction, transportation, emergency response, infrastructure inspection, and package delivery. As these vehicles approach full-autonomy, the accuracy and integrity of their navigation system become ever more stringent [1]–[4]. While the notion of accuracy is self-explanatory, the notion of integrity is less obvious, but it is of utmost importance in the safety critical application of aviation. Integrity is a criterion to evaluate the reliability and to measure the level of trust in the information produced by a navigation system. A high-integrity navigation system must be able to detect and reject faulty measurements and provide an integrity measure of the confidence in the system performance at any time. Integrity monitoring can be provided through the global navigation satellite system (GNSS) navigation messages to indicate satellite anomalies, such as clock errors. However, this type of integrity information is not useful for real-time applications, as it may take on average, about an hour (or less based on recent data), to identify and broadcast the satellite service failure. Thus, alternative frameworks for integrity monitoring have been developed, which can be categorized into internal and external [5]. External methods [e.g., ground-based augmentation system (GBAS) and satellite-based augmentation system (SBAS)] leverage a network of ground monitoring stations to monitor the transmitted signals [6], while internal methods [e.g., receiver autonomous integrity monitoring (RAIM)] typically use the redundant information within the transmitted navigation signals. RAIM inherently possesses desirable characteristics due to its design flexibility and adaptability [5]. RAIM is a technique primarily based on checking the consistency of redundant measurements. RAIM assesses the availability performance by calculating the protection level (PL) on-the-fly, which is the radius of a circular area centered around the position solution and is guaranteed to contain the true position within the specifications of RAIM, i.e., with a probability less than or equal to an acceptable integrity risk [7]. By comparing the PL with a predefined alert limit (AL), the availability of the navigation system could be determined; specifically, if the PL is less than the AL, the navigation solution is deemed reliable for the predefined integrity risk, and unreliable otherwise.

RAIM was initially proposed for GPS-based navigation. Recently, advanced RAIM (ARAIM) algorithms have been developed for multiconstellation navigation systems, which use measurements from different GNSS [8]. Nevertheless, relying on GNSS signals alone poses an alarming vulnerability for UAV navigation due to unintentional interference [9], intentional jamming [10], and spoofing [11]. Besides, due to the geometric configuration of GNSS satellites, the vertical error of the GNSS navigation solution is too large for safe UAV navigation in urban environments [12]. To account for GNSS limitations, alternative sensors have been integrated into the UAV's navigation system, and the integrity of these sensors has been the subject of recent studies. Recently, different RAIM schemes incorporating other sensing modalities have been proposed, such as i) multi-GNSS constellation RAIM (e.g., Galileo-GPS, [13] GLONASS-GPS, [8] Beidou-GPS [14], and ii) GNSS-sensor RAIM (e.g., GPS, inertial measurement units (IMUs), wheel speed encoders, and cameras [15]; GNSS-aided inertial navigation system (INS) [16]; GPS and vision [17]; GNSS and IMU [18]; GNSS, lidar, and IMU [19]; and GPS and lidar [20]).

In addition to sensors, ambient radio signals in the environment, which are not intended for navigation, have been recently considered as a supplement or an alternative to GNSS signals [21]. These signals, termed signals of opportunity (SOPs), can be terrestrial (e.g., cellular signals, digital television signals, AM/FM signals) or space-based (e.g, low Earth orbit (LEO) satellites). SOPs possess

Authors' current address: The authors are with the University of California, Irvine, CA 92697 USA (e-mail: zkassas@ieee.org).

Manuscript received 12 September 2021, revised 11 February 2022; accepted 13 May 2022, and ready for publication 9 June 2022.

Review handled by Giancarmine Fasano.

0885-8985/22/$26.00 © 2022 IEEE

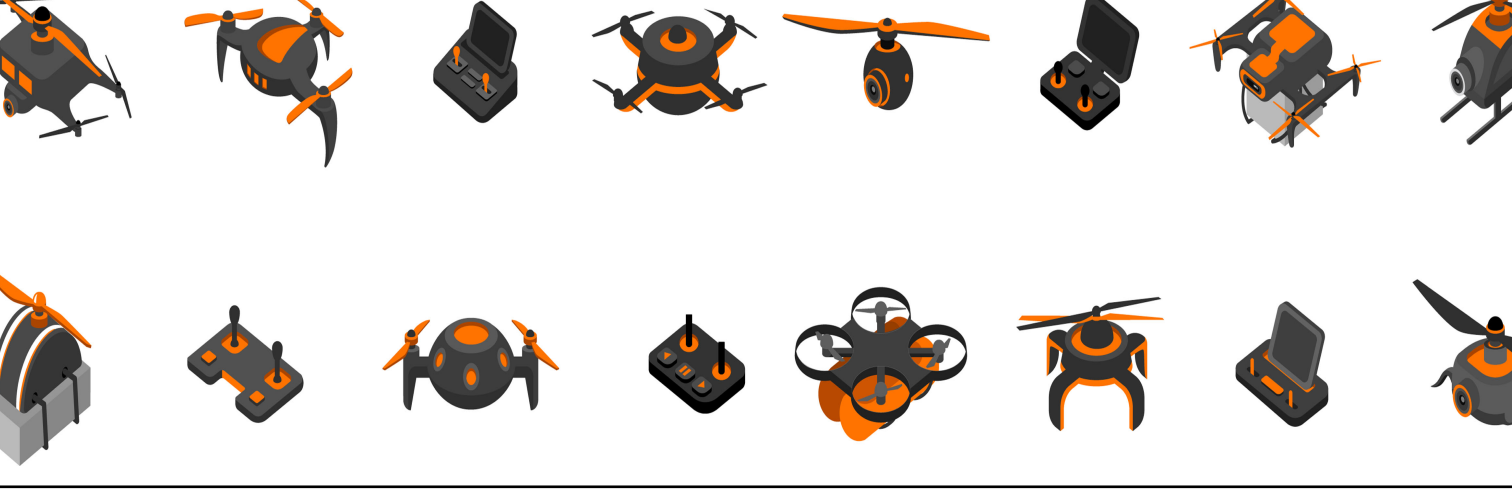

desirable characteristics for navigation purposes: i) ubiquity, ii) high received power, iii) large transmission bandwidth, iv) wide range of transmission frequencies, and v) geometric diversity. Recent research has demonstrated that cellular SOPs could yield submeter-level-accurate navigation on UAVs [22] and meter-level-accurate navigation on high altitude aircraft [23]. Moreover, it has been demonstrated that fusing GNSS and cellular SOPs results in significant reduction in the UAV's position uncertainty and PLs [12].

As the number of systems that rely on SOPs for navigation grows, the need for modeling measurement errors and monitoring the integrity of SOP-based navigation systems increases. Over the past few years, research has been conducted to model different error sources that deteriorate SOP measurements [24], [25]. In [25], it was shown that while adding more measurements from other satellites decreases the PLs, measurements from SOPs are more effective in minimizing the PL than GNSS satellites. This is due to the fact that terrestrial SOP measurements are received from negative elevation angles, as the UAV can fly above terrestrial SOPs. As a consequence, a combined GNSS-SOP system will benefit from a doubled elevation angle range. However, the integrity of SOP-based navigation systems has been barely studied in the existing literature. This article presents a new paradigm, termed opportunistic ARAIM (OARAIM), which reduces the PLs of UAVs by fusing GNSS and terrestrial SOP pseudorange measurements. It is shown that by incorporating SOPs, the PLs can be made smaller than the ones from any combination of current GNSS constellations, as shown in Figure 1. This reduction is essential in order to meet stringent integrity standard needed for safe UAV operations, especially in i) GNSS-challenged environments and ii) environments with poor satellite-to-user geometry.

Preliminary studies to assess the PL reduction due to using SOPs have been considered in [12], [24], [26]. These studies investigated a classical RAIM-based approach, where a maximum of only one measurement outlier at each time-step was considered. However, in the complicated wireless environments (e.g., deep urban canyons, nearby buildings, SOP blind spots, etc.) where the signals are heavily affected by multipath and line-of-sight-(LOS)-blockage, the assumption of experiencing only one measurement outlier may not be valid anymore. Moreover, at high altitudes [e.g., UAVs flying at an altitude of 250 m above ground level (AGL)], signal interference could be experienced [27]. To thoroughly tackle these problems, this article extends previous work through three contributions. First, in contrast to previous work, this article aims to detect more than one outlier induced into measurements due to LOS signal blockage or multipath. To this end, this article establishes a GNSS-SOP OARAIM framework and calculates the corresponding vertical PL (VPL) and horizontal PL (HPL). Second, a fault-tree and the associated fault probabilities for a combined GNSS-SOP system is developed. Then, the corresponding integrity support message (ISM) parameters for SOPs are discussed (e.g., user range error (URE), user range accuracy (URA), maximum nominal bias, etc.). Third, experimental results with cellular SOPs are presented evaluating the efficacy of the proposed OARAIM framework on a UAV for different fault conditions. A stress test shows that in faulty conditions, the OARAIM algorithm detects the faults in GPS satellites while GPS-only ARAIM fails to detect such faults. Moreover, the OARAIM algorithm reduces the gaps between the VPL and HPL and vertical and horizontal position errors (PEs) by more than 55% and 70%, respectively, compared to only using GNSS measurements.

The rest of this article is organized as follows. The section "OARAIM Framework" presents the proposed OARAIM framework. "Performance Evaluation" evaluates the performance of the OARAIM framework numerically and experimentally. Last, we present the "Conclusion."

OARAIM FRAMEWORK

This section develops the OARAIM framework to perform integrity monitoring for GNSS-SOP-based navigation. A well-designed integrity monitoring framework provides the UAV with the PLs, i.e., horizontal and vertical regions

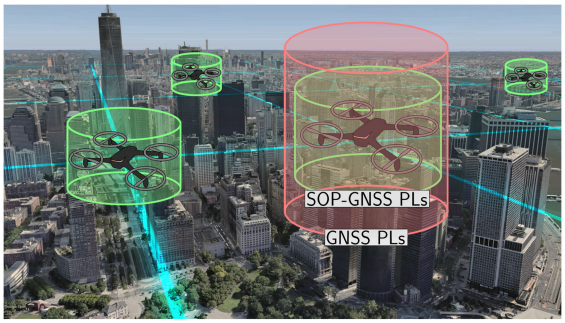

Figure 1.
UAV PLs with ARAIM (GNSS only) and OARAIM (SOP-GNSS).

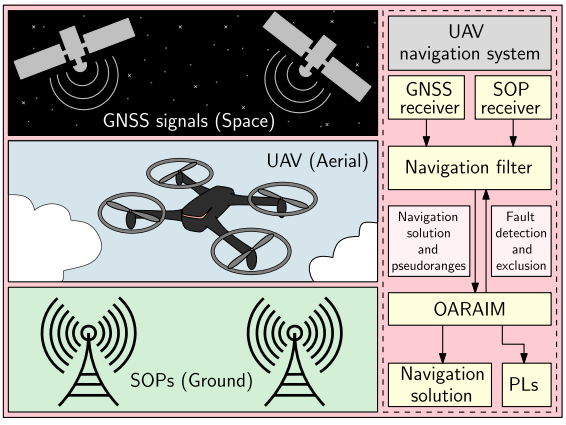

Figure 2.
Opportunistic navigation framework with OARAIM.

centered at the UAV's true position, which are guaranteed to contain the UAV's estimated position with a certain level of confidence. In this article, a baseline multiple hypothesis solution separation (MHSS) ARAIM, which was introduced in [28] is used to calculate the PLs. In the sequel, ARAIM will refer to MHSS ARAIM, for simplicity. ARAIM is a robust framework for combining navigation signals from different navigation sources with different signal properties, e.g., different URA values and different probabilities of single or multiple simultaneous faults. As such, ARAIM is well-suited for combining SOP signals with GNSS signals to form OARAIM. In addition to providing PLs, OARAIM performs fault detection and exclusion to mitigate the effect of SOP and/or GNSS system faults on the navigation solution. Figure 2 summarizes the OARAIM GNSS-SOP framework for UAV navigation.

FAULT TREE AND FAULT MODES

OARAIM operates on a fault tree. By definition, a fault tree refers to a set of assumptions about the environment in which a RAIM algorithm is applied. The measurements are supposed to be in one out of a set of different branches of the fault tree, to each of which an *a priori* probability of occurrence is assigned. Therefore, the fault tree can be employed to identify different sources of faults. OARAIM performs multiple statistical tests to detect faults, and then it attempts to exclude the detected faults. The HPL and VPL are subsequently calculated.

OARAIM considers a list of faults that need to be monitored and determines the corresponding prior probabilities that must be assigned to each mode. For simplicity, a GPS-SOP fault tree will be discussed. Extension to other GNSS constellations is expected to be straightforward. In [28], a method was presented to determine the faults that need to be monitored and the associated probabilities of faults. Using the same methodology, in this article, a maximum of three simultaneous faults are considered. Also, the probability of a constellation fault (i.e., a fault that affects all transmitters) for both GPS and SOP transmitters are assumed to be sufficiently improbable. This assumption relies on historical record of these signals. GPS records show that there is no evidence of a constellation fault since the first GPS satellites were launched [29]. Moreover, no SOP "constellation" faults were experienced in any of the tests performed in [25]; however, since there is not enough SOP data to compute this probability yet, this may be an optimistic assumption. The resulting GPS-SOP fault tree is depicted in Figure 3. It is assumed that the true SOP "constellation" fault will not change the number of faults to be monitored in the current fault tree. In the case that the number of faults change, the fault tree should be updated accordingly

To calculate the mode probabilities, the probability of GPS satellite and SOP transmitter failures must be known, namely $\{P_{\text{GPS},i}\}_{i=1}^{N_{\text{GPS}}}$ and $\{P_{\text{SOP},i}\}_{i=1}^{N_{\text{SOP}}}$, respectively; where N_{GPS} and N_{GPS} are the numbers of visible GPS satellites and SOP transmitters, respectively. In this article, all SOP transmitter failure probabilities were set to $\{P_{\text{SOPi},i}\}_{i=1}^{N_{\text{SOP}}} = P_{\text{SOP}} = 10^{-4}$ and all GPS satellite failure probabilities were set to $\{P_{\text{GPS},i}\}_{i=1}^{N_{\text{GPS}}} = P_{\text{GPS}} = 10^{-5}$, according to the historical records detailed in [30]. The choice of P_{SOP} is discussed in the Experimental Results section. Subsequently, the GPS-SOP fault probability for Mode n can be expressed as

$$P_{\text{Mode},n} = \binom{N_{\text{GPS}}}{k_{\text{GPS},n}} P_{\text{GPS}}^{k_{\text{GPS},n}} (1-P_{\text{GPS}})^{(N_{\text{GPS}}-k_{\text{GPS},n})} \cdot \binom{N_{\text{SOP}}}{k_{\text{SOP},n}} P_{\text{SOP}}^{k_{\text{SOP},n}} (1-P_{\text{SOP}})^{(N_{\text{SOP}}-k_{\text{SOP},n})} \quad (1)$$

where $n = 0, \ldots, 10$, is the mode index and $k_{\text{GPS},n}$ and $k_{\text{SOP},n}$ are the number of faulty GPS satellites and SOP transmitters in Mode n, respectively. Modes 1 to 9 correspond to the faulty operations, including one, two, and three simultaneous faults, while Mode 10 is assumed to never occur.

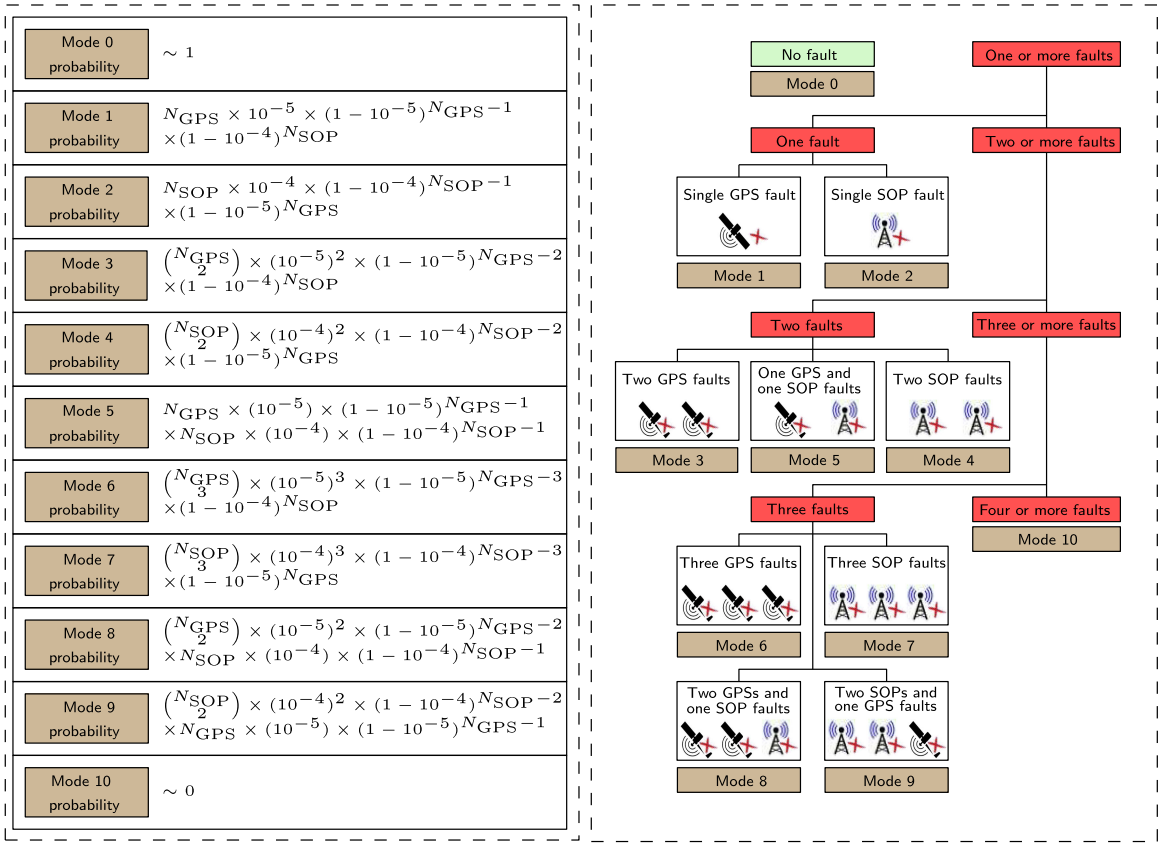

Figure 3.
GPS-SOP fault tree and the associated probabilities calculated according to (1).

OARAIM ALGORITHM

OARAIM shares some common inputs and constant parameters used by ARAIM [28]. While some values are independent of the signal type (e.g., total integrity budget, probability of false alarm, etc.), other values are SOP-specific. The ORAIM inputs are tabulated in Table 1. In contrast to traditional RAIM frameworks, where pseudorange measurement errors are assumed to have zero-mean, ARAIM accounts for unknown but bounded pseudorange biases denoted by $\{b_{\mathrm{nom,GPS},i}\}_{i=1}^{N_{\mathrm{GPS}}}$. For GPS measurements, these biases bound nominal errors, mainly due to the code correlation peak deformation [31]. The values of the biases are extracted from the ISM and can be limited to 0.75 m [5]. A similar value can be conservatively used for biases in SOP measurements, denoted by $\{b_{\mathrm{nom,SOP},i}\}_{i=1}^{N_{\mathrm{SOP}}}$, as SOP signals are unaffected by atmospheric errors.

A summary of the OARAIM algorithm is given below. The steps below highlight the differences between the ARAIM and OARAIM algorithm. The details of the ARAIM algorithm can be found in [28].

Step 1: Compute the pseudorange error covariance matrices denoted $\mathbf{C}_{\mathrm{int}}$ and $\mathbf{C}_{\mathrm{acc}}$, where the former is computed using the URA standard deviations $\{\sigma_{\mathrm{URA,GPS},i}\}_{i=1}^{N_{\mathrm{GPS}}}$ and $\{\sigma_{\mathrm{URA,SOP},i}\}_{i=1}^{N_{\mathrm{SOP}}}$, and the latter using the URE standard deviations $\{\sigma_{\mathrm{URE,GPS},i}\}_{i=1}^{N_{\mathrm{GPS}}}$ and $\{\sigma_{\mathrm{URE,SOP},i}\}_{i=1}^{N_{\mathrm{SOP}}}$. Without loss of generality, it is assumed that the combined GPS-SOP measurements are ordered as GPS measurements first then SOP. The diagonal elements of $\mathbf{C}_{\mathrm{int}}$ and $\mathbf{C}_{\mathrm{acc}}$ pertaining to GPS satellites are calculated according to, [28] and the ones pertaining to SOPs are given by

$$\mathbf{C}_{\mathrm{int}}(N_{\mathrm{GPS}}+i, N_{\mathrm{GPS}}+i) = \sigma^2_{\mathrm{URA,SOP},i} \tag{2}$$

$$\mathbf{C}_{\mathrm{acc}}(N_{\mathrm{GPS}}+i, N_{\mathrm{GPS}}+i) = \sigma^2_{\mathrm{URE,SOP},i}, \tag{3}$$

for $i = 1, \ldots, N_{\mathrm{SOP}}$.

Step 2: Compute the all-in-view position solution using weighted least-squares estimation with weight matrix $\mathbf{C}_{\mathrm{int}}^{-1}$. All available GNSS and SOP measurements are used in this step.

Step 3: Determine the fault modes, which are the faults that need to be monitored and their associated probabilities. These modes for the OARAIM algorithm are summarized in the fault tree shown in Figure 3.

Step 4: Evaluate the fault-tolerant positions and associated standard deviations and biases for each fault mode. A fault-tolerant position for a certain mode is computed using all measurements except the measurements of the assumed faulty GNSS satellites or SOPs in that given

Table 1.

Inputs to the GPS-SOP OARAIM Algorithm		
Input	Description	Obtained from
$\{z_{\text{GPS,i}}\}_{i=1}^{N_{\text{GPS}}}$	GPS pseudorange measurements	GPS front-end and tracking loop
$\{z_{\text{SOP,i}}\}_{i=1}^{N_{\text{SOP}}}$	SOP pseudorange measurements	SOP front-end and tracking loop
$\{\sigma_{\text{URA,GPS,i}}\}_{i=1}^{N_{\text{GPS}}}$	Standard deviation of GPS user range accuracy	ISM
$\{\sigma_{\text{URA,SOP,i}}\}_{i=1}^{N_{\text{SOP}}}$	Standard deviation of SOP user range accuracy	The value of URE multiplied by 1.5
$\{\sigma_{\text{URE,GPS,i}}\}_{i=1}^{N_{\text{GPS}}}$	Standard deviation of the GPS user range error	ISM
$\{\sigma_{\text{URE,SOP,i}}\}_{i=1}^{N_{\text{SOP}}}$	Standard deviation of the SOP user range error	[25]
$\{b_{\text{nom,GPS,i}}\}_{i=1}^{N_{\text{GPS}}}$	Maximum bias for a GPS measurement	ISM
$\{b_{\text{nom,SOP,i}}\}_{i=1}^{N_{\text{SOP}}}$	Maximum bias for a SOP measurement	Similar to the GPS maximum bias
$\{P_{\text{GPS,i}}\}_{i=1}^{N_{\text{GPS}}}$	Probability of a single GPS fault	Historical records. Currently used value is 10^{-5}
$\{P_{\text{SOP,i}}\}_{i=1}^{N_{\text{SOP}}}$	Probability of a single SOP fault	Experimental campaign. Proposed value is 10^{-4}
$P_{\text{Const,GPS}}$	Probability of GPS constellation fault	Historical records. Currently used value is 0
$P_{\text{Const,SOP}}$	Probability of SOP constellation fault	Experimental campaign. Proposed value is 0

mode. In particular, this step derives the following parameters for each fault mode:

The variances of the fault-tolerant position components (East, North, Up) for each fault mode.

The difference between the fault-tolerant position and the all-in-view position and the variance of this difference.

The worst-case impact of the nominal biases $\{b_{\text{nom,GPS},i}\}_{i=1}^{N_{\text{GPS}}}$ and $\{b_{\text{nom,SOP},i}\}_{i=1}^{N_{\text{SOP}}}$ on the position estimate.

Step 5: Perform two sets of tests:

Solution separation tests:

- Compute the solution separation test thresholds from the probability of false alarm.
- Perform the test on all the components of the difference between the fault-tolerant and all-in-view solutions for each fault mode. If any test fails, exclusion must be attempted.

A chi-squared test:

- A chi-squared test is performed on the measurement residuals for the all-in-view solution with weight matrix $\mathbf{C}_{\text{acc}}$ calculated in **Step 1**.
- The threshold is computed using the inverse chi-squared cumulative density function (cdf) and a pre-defined probability of false alarm.
- If the chi-squared test fails, the PLs cannot be considered valid and exclusion cannot be attempted. If this test fails while none of the solution separation tests fail, then the fault is most likely outside the threat model. The chi-square test is a sanity check for that purpose.

Step 6: Calculate the PLs if all of the solution separation tests and the chi-squared test pass and formulate the vertical positioning performance criteria:

1) Criterion 1: 95% accuracy parameter, which is the achievable positioning accuracy in the vertical domain 95% of the time. According to the Localizer Performance with Vertical guidance (LPV)- 200 standard, the 95% accuracy must be limited to 4 m.
2) Criterion 2: 10^{-7} fault-free position error bound, which is the achievable positioning accuracy in the vertical domain 99.99999% of the fault-free time. According to the LPV-200 standard, the 10^{-7} fault-free position error bound must be limited to 10 m.
3) Criterion 3: Effective monitor threshold (EMT), which is a parameter that takes into account the faults with a prior greater than or equal to 10^{-5}. According to the LPV-200 standard, EMT must be limited to 15 m.

If the chi-squared test passes but any of the solution separation tests fail, the following steps are performed instead.

Step 7: Exclude the faults by first determining the candidate subset to exclude. This is achieved by performing a search over all possible subsets to find the subset that yields the highest discrepancy between the fault-tolerant and all-in-view solution. Once the best candidate subset is determined, an exclusion test is performed to account for the wrong exclusion probability.

Step 8: Compute the PLs after exclusion. This step is similar to **Step 6** except that it accounts for the wrong exclusion probability.

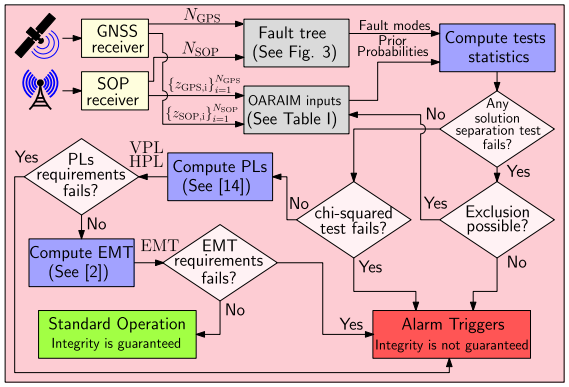

Figure 4.
OARAIM algorithm.

Step 9: Compute the 95% accuracy criterion after exclusion to account for fault modes.

Remark: Note that the above used LPV-200 requirements, which were developed for aircraft operation, since no formal integrity requirements established for small UAVs as of yet. As stakeholders develop such requirements for UAVs, the parameters in the OARAIM algorithm can be adjusted accordingly.

Figure 4 summarizes the proposed OARAIM algorithm.

PERFORMANCE EVALUATION

This section evaluates the performance of the OARAIM framework numerically and experimentally. The OARAIM algorithm was implemented using the MATLAB Algorithm Availability Simulation Tool (MAAST) [29], [32].

SIMULATION RESULTS

In order to study the performance of the OARAIM algorithm under fault-free and faulty conditions, a simulation was performed with two SOPs. For this test, GPS signals were obtained from a stationary receiver at the Madrid Deep Space Communications Complex (MDSCC). The elevation and azimuth angles of the GPS satellite constellation above the receiver over a 24-h period was computed using GPS ephemeris files collected at the MDSCC. The GPS observations were extracted from the recorded Receiver Independent Exchange Format (RINEX) file. Then, the SOP signals were simulated using a high-fidelity SOP simulator that has been used in previous research [24]. The SOP and receiver's clock qualities were modeled as typical oven-controlled crystal oscillator (OCXO) and temperature-compensated crystal oscillator (TCXO), respectively. To overcome the unknown nature of the SOP transmitter's clock bias and its drift, which in GNSS-based navigation are known through the navigation message, a reference receiver, referred to as the base, is assumed to be present in the UAV's environment to provide differential corrections. Moreover, it is assumed that the base has direct line-of-sight (LOS) to all of the cellular towers to eliminate the possibility of common errors. The impact of using a base receiver on an SOP-based integrity monitoring framework has been fully investigated in [24], where a base receiver was employed to estimate the SOP clock biases through a Kalman filter. Considering that the base receiver could be deployed on top of a building, it can be assumed that it has access to unobstructed GNSS signals from which it can estimate its own clock bias. Hence, for the purpose of this study, it is assumed that the base has complete knowledge of its position and its clock bias and that it does not introduce a nonzero mean common mode error in the UAV's differential measurements. Once the measurements are corrected, a common clock bias term remains to be estimated, and is added to the set of constellation clock biases to be estimated.

In the first scenario, both SOPs were fault-free. In the second scenario, a fault of a magnitude of 30 m was injected into the second SOP measurement. To illustrate the accuracy and integrity performances simultaneously, a so-called Stanford diagram was plotted in Figure 5, where PE, PL, and AL are shown for four scenarios: GPS-only (black dots), GPS-SOP in fault-free operation (blue dots), GPS-SOP without OARAIM fault exclusion (red dots), and GPS-SOP with OARAIM fault exclusion (blue dots). The AL was set to 30 m.

Note that except for the red points, the PLs in Figure 5 are calculated only after tests have passed, or after exclusion in the case where faults are detected. However, similar to [7], the PLs before exclusion (red) are shown in the Stanford plot for a comparative analysis. The following may be

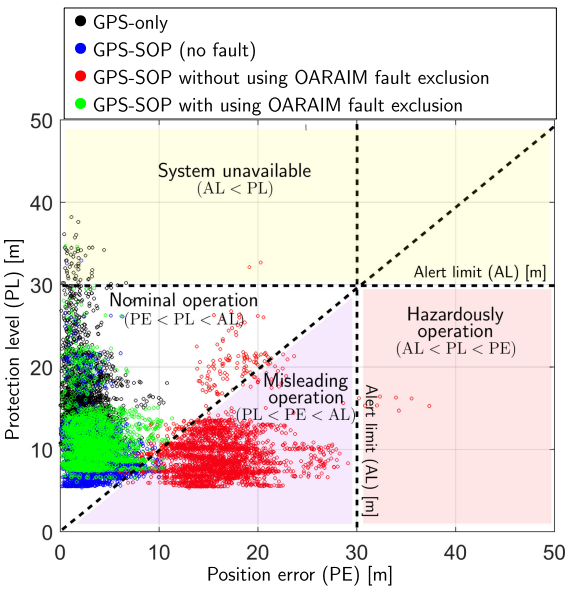

Figure 5.
The Stanford diagram demonstrating the horizontal accuracy and integrity performances simultaneously.

concluded from Figure 5. First, by comparing the blue and black dots, it can be seen that adding SOPs eliminates system unavailability. Second, injecting the fault into an SOP measurement caused a misleading operation (red dots); however, the OARAIM algorithm rejected the faulty measurement to achieve nominal operation (green dots). Third, by comparing the red and green dots, it can be seen that as expected, fault exclusion results in reducing the PE. However, one can spot green and blue dots in the misleading operation region. With only two SOPs, the integrity system will heavily couple the GPS and SOP "constellations" since there are not enough SOPs to compute an SOP-only position solution. This could explain the occasional green or blue point in the misleading operation region. However, one can see that the PL is reduced on average when SOPs are used with GPS for integrity, as shown by the lowered green and blue cloud points compared to the GPS's black point cloud.

EXPERIMENTAL RESULTS

In order to evaluate the performance of the proposed OARAIM framework in a real-world scenario, a DJI Matrice 600 UAV was equipped with a dual-channel National Instrument (NI) universal software radio peripheral (USRP)-2955 to sample cellular long-term evolution (LTE) SOPs at four LTE carrier frequencies: 739, 1955, 2125, and 2145 MHz. These frequencies are allocated for the U.S. cellular providers AT&T, T-Mobile, and Verizon. The ground-truth reference for the UAV's trajectory was taken from a Septentrio AsteRx-i V integrated GNSS-IMU system, which is capable of producing a submeter-level accurate real-time kinematic (RTK) navigation solution. Figure 6 shows the experimental hardware and software setup and Figure 7 shows the experimental environment.

The UAV flew for 4 min, while collecting LTE signals from 11 LTE SOP transmitters in the environment. The stored LTE signals were then processed by the LTE module of the Multichannel Adaptive Transceiver Information eXtractor (MATRIX) SDR to produce LTE SOP pseudoranges, which were then fused with GPS pseudorange measurements obtained from the Septentrio receiver to produce the navigation solution along with the corresponding OARAIM integrity measures, as shown in Figure 7.

Two scenarios were considered to evaluate the impact of SOP measurements on navigation and safety: (i) fault-free conditions and (ii) faulty conditions with faults in two GPS satellites. The faults were injected artificially as a stress test for the OARAIM and ARAIM frameworks in postprocessing in the form of 10 m biases in the pseudorange measurements from GPS PRN 5 and PRN 25 over a period of 1 min. For each scenario, two sets of results are computed: (a) a navigation solution and ARAIM integrity measures using GPS measurements only and (b) a navigation solution and OARAIM integrity measures using GPS and cellular

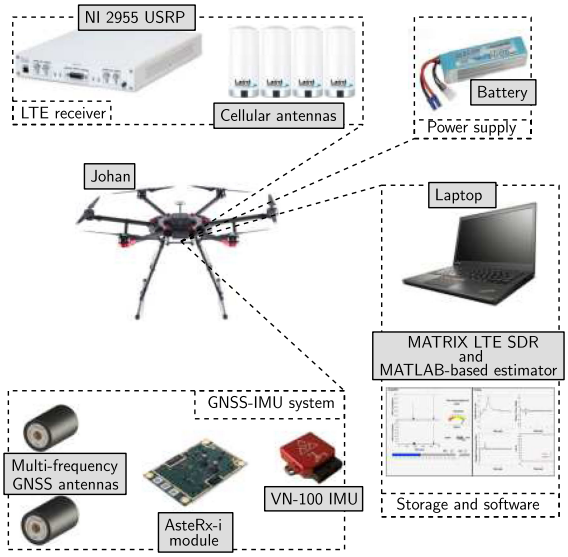

Figure 6.
Experimental hardware and software setup.

LTE SOP measurements. A very preliminary study characterizing the measurement statistics of cellular SOPs shows that $\sigma_{\mathrm{URE,SOP},i}$ is around 0.75 m at high altitudes in a semiurban environment [12]. While the UAV is flown in a similar environment in this article, this value of $\sigma_{\mathrm{URE,SOP},i}$ was inflated by 25% to be more conservative. As such, the ARAIM and OARAIM algorithms were implemented with $\sigma_{\mathrm{URA,GPS},i} = 1.1$ m, $\sigma_{\mathrm{URE,GPS},i} = 0.75$ m, $\sigma_{\mathrm{URA,SOP},i} = 1.4$ m, $\sigma_{\mathrm{URE,SOP},i} = 0.9375$ m, $\{b_{\mathrm{nom,GPS},i}\}_{i=1}^{N_{\mathrm{GPS}}} = 0.5$ m, and $\{b_{\mathrm{nom,SOP},i}\}_{i=1}^{N_{\mathrm{SOP}}} = 0.75$ m, for all i. Moreover, it was found in[12] that the measurement error for UAV flights is less than 5.42 m. Using this standard deviation as a definition of a fault at high altitude in a semiurban environment yields an SOP fault probability of about 10^{-4} (corresponding to $3.89\sigma_{\mathrm{URA,SOP},i}$). Therefore, the prior satellite fault probabilities were set to 10^{-5} and the prior SOP fault probabilities were set to 10^{-4}, with zero probability for constellation faults. The $\sigma_{\mathrm{URE,SOP},i}$ and $\sigma_{\mathrm{URA,SOP},i}$ values are relatively low since cellular signals received by UAVs do not suffer from severe multipath by virtue of the favorable channel between base stations and UAVs. In fact, a recent study of UAV connectivity to the cellular network demonstrated that the received cellular signal power on low-altitude UAVs (30 m to 120 m) are stronger than the receiver power on ground-based receivers, despite the downward-tilted cellular antennas[33]. The study attributes these findings to the fact that "free space propagation conditions at altitude more than make up for antenna gain reductions." It is important to note that the reliability of cellular SOP has not been fully characterized yet. As such, a 10^{-4} fault probability could be either conservative or optimistic. However, in the case of the latter, it has been shown in [34] that OARAIM would still yield improvement over

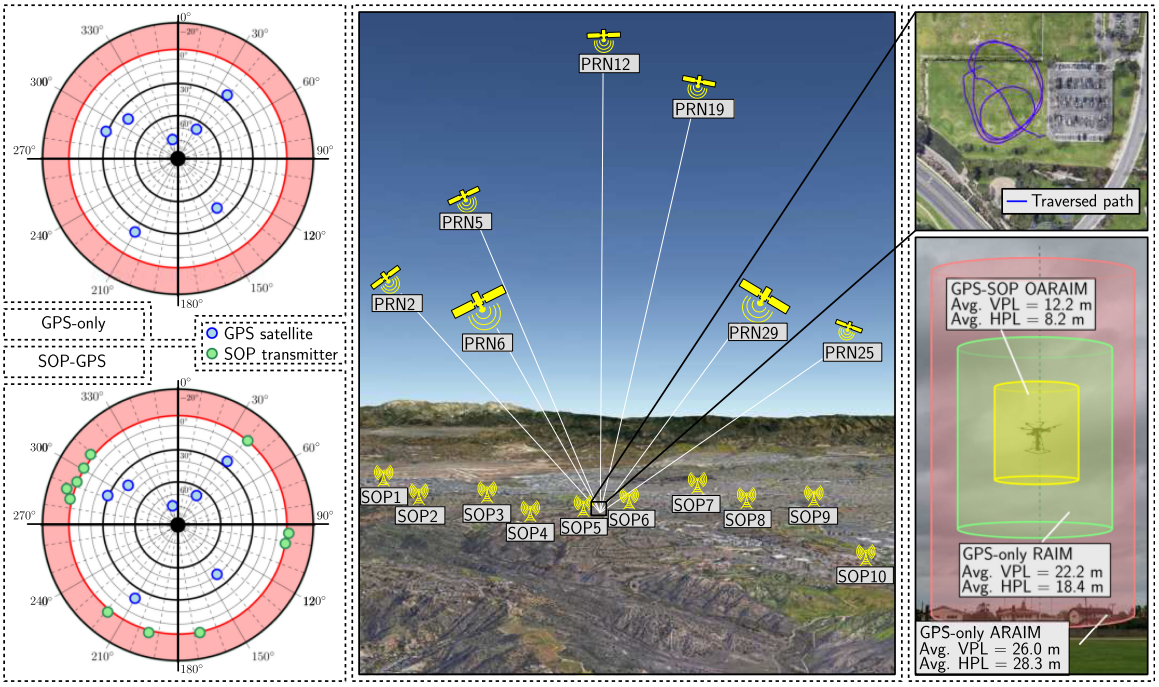

Figure 7.
Experimental environment, experimental setup, and experimental results showing the traversed trajectory, the GPS-only and SOP-GPS sky-plots showing satellite-to-user and SOP transmitter-to-user geometry. The average fault-free PLs across the entire trajectory using GPS-only RAIM, GPS-only ARAIM, and GPS-SOP OARAIM are plotted for comparison.

ARAIM for high and unlikely SOP fault probabilities of 10^{-2}.

One important integrity functionality studied in these experiments is fault detection. Figure 8 shows the chi-squared test results for the GPS-only and GPS-SOP systems in fault-free and faulty conditions. The main takeaway from Figure 8 is that although the test threshold increases by adding SOP measurements (a straightforward property of chi-squared-distributed random variables), the test statistic itself becomes more sensitive to faults. This also

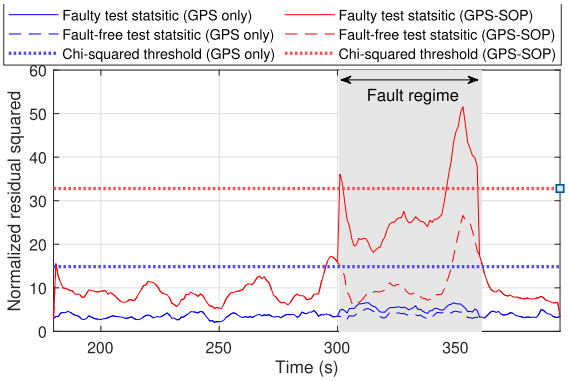

Figure 8.
Time history of the chi-squared test statistic for GPS-only and GPS-SOP with their respective test thresholds. The test-statistic for each system are shown in fault-free and faulty conditions. The shaded area represents faulty conditions.

applies to the solution separation tests, which are not shown here for brevity. No faults were detected by the GPS-only ARAIM system in the fault regime, whereas the GPS-SOP OARAIM system detected such faults. It is worth pointing out that while Figure 8 studied the chi-squared test results, studying the solution separation test results would yield a large number of cases, which is deferred to future work.

Next, the gap between the HPL and the horizontal position error (HPE), and the gap between the VPL and vertical position error (VPE) were studied. The gap between PLs and PEs is an indicator of the tightness of the PLs. The gaps are calculated according to $\Delta V \triangleq VPL - VPE$ and $\Delta H \triangleq HPL - HPE$. The root mean-squared error (RMSE) of ΔV and ΔH were computed for both GPS-only and GPS-SOP and in fault-free and faulty conditions. The results are tabulated in Table 2 and Figure 9.

The following can be concluded from Table 2 and Figure 9. First, ΔH and ΔV are reduced significantly when SOP measurements are added, with more than 70% reduction in the ΔH RMSE and more than 55% in the ΔV RMSE. Figure 9 shows that while the PLs were significantly reduced, the PEs slightly reduce as well. This implies that adding SOP measurements significantly tighten the PLs toward the PEs without the PEs exceeding the PL. This is a desirable behavior as it moves the system more to the left of the "Nominal operation" region shown in Figure 5. Second, the change in the ΔH RMSE between fault-free and faulty conditions for

Table 2.

RMSE Values of ΔH and ΔV for GPS-Only ARAIM and GPS-SOP ARAIM in Fault-Free and Faulty Conditions

Approach	Condition	ΔH RMSE	ΔV RMSE
GPS-only ARAIM	Fault-free	26.9 m	24.7 m
GPS-SOP OARAIM	Fault-free	7.5 m	11.0 m
GPS-only ARAIM	Faulty	25.3 m	24.8 m
GPS-SOP OARAIM	Faulty	7.6 m	11.4 m

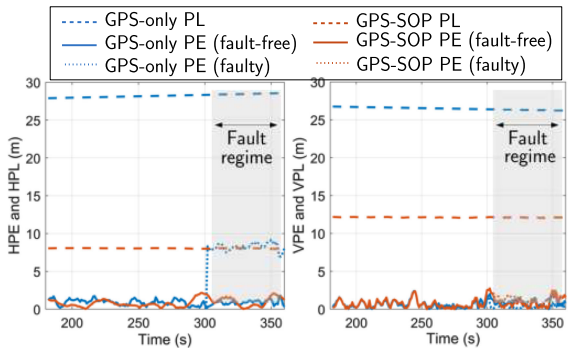

Figure 9.
The PE versus PL values for GPS-only ARAIM and GPS-SOP OARAIM in fault-free and faulty conditions.

GPS-only is much greater than the change for the GPS-SOP, i.e., around 6% compared to 1.3%, respectively. The reduction in the GPS-only ΔH RMSE is due to the HPEs getting larger because of the undetected faults while the HPL remained unchanged. This undesirable behavior brings the system closer to the "Misleading operation" region of Figure 5. In the case of GPS-SOP, the faults are detected and excluded properly, maintaining low ΔH and ΔV RMSEs in the presence of faults. It is important to note that in this particular experiment, the VPL is lower than the HPL in the case of GPS-only, as shown in Figure 9. This may be due to the fact the probability of hazardous misleading information (PHMI) for the VPL is about 100 times the PHMI for the HPL when using standard ARAIM parameters from the GPS ISM, as shown in Table 1. However, the ARAIM system does not necessarily need to detect the faults with high probability. In this study, both the GPS-SOP OARAM and the GPS-only ARAIM algorithms were set up with standard ISM values shown in Table 1 for a comparative analysis. Tuning and designing the OARAIM and ARAIM parameters for optimal performance is left for future work.

Remark: While the presented simulation and experiment results look promising, they are not enough to generalize the conclusions. They provide an insight into the potential of SOPs in improving integrity monitoring. Extensive simulations and experiments are needed to generalize the results obtained in this article and are left as future work.

CONCLUSION

To improve the availability of the integrity monitoring system, the capability to detect faults must be improved and PLs must remain small. This article showed that by incorporating SOPs, the fault detection probability is increased and PLs can be made smaller than the ones from current GNSS constellations. To this end, the article presented an OARAIM framework for enhanced UAV safety. OARAIM enables safe UAV navigation by fusing GNSS signals with ambient SOPs, producing tight PLs, while identifying and excluding faults, if present. A fault tree was constructed for GPS-SOP-based navigation and the OARAIM algorithm was presented. Simulation results were presented demonstrating that adding SOPs eliminates system unavailability of the integrity system. Experimental results were presented showing that in faulty conditions, the OARAIM algorithm detects the faults in GPS satellites while GPS-only ARAIM failed to detect such faults. Moreover, the OARAIM algorithm reduces the gaps between vertical and horizontal PLs and PEs by more than 55% and 70%, respectively, compared to only using GNSS measurements. The PL reduction in OARAIM translates to higher availability of the integrity monitoring system, allowing the UAV navigation system to meet more stringent integrity standards than ARAIM with GNSS only.

ACKNOWLEDGMENTS

The authors would like to thank Kimia Shamaei for her help in data collection. This work was supported in part by the National Science Foundation (NSF) under Grant 1929965, in part by the Office of Naval Research (ONR) under Grant N00014-19-1-2613, and in part by the U.S. Department of Transportation (USDOT) under Grant 69A3552047138 for the CARMEN University Transportation Center (UTC).

REFERENCES

[1] R. Loh, Y. Bia, and T. Roe, "UAVs in civil airspace: Safety requirement," *IEEE Aerosp. Electron. Syst. Mag.*, vol. 24, no. 1, pp. 5–17, Jan. 2009.

[2] Z. Kassas, P. Closas, and J. Gross, "Navigation systems for autonomous and semi-autonomous vehicles: Current trends and future challenges," *IEEE Aerosp. Electron. Syst. Mag.*, vol. 34, no. 5, pp. 82–84, May 2019.

[3] R. Sabatini *et al.*, "Avionics systems panel research and innovation perspectives," *IEEE Aerosp. Electron. Syst. Mag.*, vol. 35, no. 12, pp. 58–72, Dec. 2020.

[4] "NextGen annual report: A report on the history, current status, and future of national airspace system modernization," U.S. Dept. Transp., Federal Aviation Administration, 2020, pp. 1–154.

[5] V. Kropp, "Advanced receiver autonomous integrity monitoring for aircraft guidance using GNSS," Ph.D. dissertation, Univ. of Munich, Munich, Germany, 2018.

[6] R. Sabatini, T. Moore, and C. Hill, "Avionics-based GNSS integrity augmentation synergies with SBAS and GBAS for safety-critical aviation applications," in *Proc. IEEE/AIAA Digit. Avionics Syst. Conf.*, 2016, pp. 1–10.

[7] S. Bhattacharyya and D. Gebre-Egziabher, "Kalman filter-based RAIM for GNSS receivers," *IEEE Trans. Aerosp. Electron. Syst.*, vol. 51, no. 3, pp. 2444–2459, Jul. 2015.

[8] T. Walter, J. Blanch, M. J. Choi, T. Reid, and P. Enge, "Incorporating GLONASS into aviation RAIM receivers," in *Proc. Int. Tech. Meeting Inst. Navigation*, 2013, pp. 239–249.

[9] C. Hegarty, D. Bobyn, J. Grabowski, and A. Van Dierendonck, "An overview of the effects of out-of-band interference on GNSS receivers," *J. Inst. Navigation*, vol. 67, no. 1, pp. 143–161, Mar. 2020.

[10] D. Borio, F. Dovis, H. Kuusniemi, and L. Presti, "Impact and detection of GNSS jammers on consumer grade satellite navigation receivers," *Proc. IEEE*, vol. 104, no. 6, Jun. 2016, pp. 1233–1245.

[11] C. Günther, "A survey of spoofing and counter-measures," *J. Inst. Navigation*, vol. 61, no. 3, pp. 159–177, 2014.

[12] M. Maaref, J. Khalife, and Z. Kassas, "Aerial vehicle protection level reduction by fusing GNSS and terrestrial signals of opportunity," *IEEE Trans. Intell. Transp. Syst.*, vol. 22, no. 9, pp. 5976–5993, Sep. 2021.

[13] A. Ene, J. Blanch, and T. Walter, "Galileo-GPS RAIM for vertical guidance," in *Proc. Nat. Tech. Meeting Inst. Navigation*, 2006, pp. 18–20.

[14] Y. Liu and Y. Zhu, "Design and performance evaluation of airspace-ground cooperative GPS/BeiDou dual-constellation RAIM algorithm," in *Proc. ION Int. Tech. Meeting*, 2014, pp. 127–136.

[15] R. Toledo-Moreo, D. Betaille, and F. Peyret, "Lane-level integrity provision for navigation and map matching with GNSS, dead reckoning, and enhanced maps," *IEEE Trans. Intell. Transp. Syst.*, vol. 11, no. 1, pp. 100–112, Mar. 2010.

[16] O. Garcia Crespillo, A. Grosch, B. Belabbas, and M. Rippl, "GNSS-aided INS integrity concept," in *Proc. 27th Int. Techn. Meeting Satell. Division Inst. Navigation*, 2014, pp. 2069–2077.

[17] L. Fu, J. Zhang, R. Li, X. Cao, and J. Wang, "Vision-aided RAIM: A new method for GPS integrity monitoring in approach and landing phase," *Sensors*, vol. 15, no. 9, pp. 22854–22873, 2015.

[18] T. Needham and M. Braasch, "Gravity model error considerations for high-integrity GNSS-aided INS operations," in *Proc. IEEE/ION Position, Location, Navigation Symp.*, 2018, pp. 822–832.

[19] A. Hassani, N. Morris, M. Spenko, and M. Joerger, "Experimental integrity evaluation of tightly-integrated IMU/LiDAR including return-light intensity data," in *Proc. 32nd Int. Techn. Meeting Satell. Division Inst. Navigation*, 2019, pp. 2637–2658.

[20] T. Li *et al.*, "P3-LOAM: PPP/LiDAR loosely coupled SLAM with accurate covariance estimation and robust RAIM in urban canyon environment," *IEEE Sensors J.*, vol. 21, no. 5, pp. 6660–6671, Mar. 2021.

[21] J. Raquet *et al.*, "Position, navigation, and timing technologies in the 21st century," *Part D: Position, Navigation, and Timing Using Radio Signals-of-Opportunity*, vol. 2. J. Morton, F. van Diggelen, J. Spilker, Jr., and B. Parkinson, Eds. Hoboken, NJ, USA: Wiley-IEEE, 2021, ch. 35–43, pp. 1115–1412.

[22] J. Khalife and Z. Kassas, "On the achievability of submeter-accurate UAV navigation with cellular signals exploiting loose network synchronization," *IEEE Trans. Aerosp. Electron. Syst.*, early access, Mar. 31, 2022, doi: 10.1109/TAES.2022.3162770.

[23] Z. Kassas *et al.*, "Assessment of cellular signals of opportunity for high altitude aircraft navigation," *IEEE Aerosp. Electron. Syst. Mag.*, early access, Jun. 29, 2022, doi: 10.1109/MAES.2022.3187142.

[24] M. Maaref and Z. Kassas, "Measurement characterization and autonomous outlier detection and exclusion for ground vehicle navigation with cellular signals," *IEEE Trans. Intell. Veh.*, vol. 5, no. 4, pp. 670–683, Dec. 2020.

[25] M. Maaref and Z. Kassas, "Autonomous integrity monitoring for vehicular navigation with cellular signals of opportunity and an IMU," *IEEE Trans. Intell. Transp. Syst.*, vol. 23, no. 6, pp. 5586–5601, Jun. 2022.

[26] M. Maaref, J. Khalife, and Z. Kassas, "Enhanced safety of autonomous driving by incorporating terrestrial signals of opportunity," in *Proc. IEEE Int. Conf. Acoust., Speech, Signal Process.*, 2020, pp. 9185–9189.

[27] A. Colpaert, E. Vinogradov, and S. Pollin, "Aerial coverage analysis of cellular systems at LTE and mmWave frequencies using 3D city models," *Sensors*, vol. 18, no. 12, Dec. 2018, Art. no. 4311.

[28] J. Blanch *et al.*, "Advanced RAIM user algorithm description: Integrity support message processing, fault detection, exclusion, and protection level calculation," in *Proc. 25th Int. Tech. Meeting Satell. Division Inst. Navigation*, 2012, pp. 2828–2849.

[29] "Advanced RAIM technical subgroup reference airborne algorithm description document," 3rd Generation Partnership Project (3GPP), Working Group-C, Tech. Rep., Jun. 2019. [Online]. Available: http://web.stanford.edu/group/scpnt/gpslab/website_files/maast/ARAIM_TSG_Reference_ADD_v3.1.pdf

[30] T. Walter and J. Blanch, "Characterization of GNSS clock and ephemeris errors to support ARAIM," in *Proc. ION Pacific PNT Meeting, Conf.*, 2015, pp. 920–931.

[31] D. Imparato, "GNSS-based receiver autonomous integrity monitoring for aircraft navigation," Ph.D. dissertation, Delft Univ. of Technol., CD Delft, Netherlands, 2016.

[32] J. Shau, W. Chan, and T. Walter, "MATLAB algorithm availability simulation tool," *GPS Solutions*, vol. 13, pp. 327–332, 2009.

[33] "LTE unmanned aircraft systems," QualcommTechnologies Inc., Tech. Rep. 1.0.1, May 2017. [Online]. Available: https://www.qualcomm.com/documents/lte-unmanned-aircraft-systems-trial-report/

[34] M. Jia, J. Khalife, and Z. Kassas, "Evaluation of ground vehicle protection level reduction due to fusing GPS with faulty terrestrial signals of opportunity," in *Proc. ION Int. Tech. Meeting*, 2021, pp. 354–365.